

Article

Development of Non-Spherical Platinum Nanoparticles on Carbon Supports for Oxygen Reduction Reaction

Mark Lim ¹, Mohmmad Khalid ², Samaneh Shahgaldi ^{1,2} and Xianguo Li ^{1,*}

¹ Department of Mechanical and Mechatronics Engineering, University of Waterloo, Waterloo, ON N2L 3G1, Canada; m26lim@uwaterloo.ca (M.L.); samaneh.shahgaldi@uqtr.ca (S.S.)

² Institute of Eco-Materials, Eco-Products and Eco-Energies (I2E3), University of Quebec at Trois-Rivieres (UQTR), Trois-Rivieres, QC G8Z 4M3, Canada; mohmmad.khalid@uqtr.ca

* Correspondence: xianguo.li@uwaterloo.ca

Abstract: Proton exchange membrane fuel cells are anticipated to play an important role in decarbonizing the global energy system, but the performance of platinum (Pt) catalysts must be improved to make this technology more economical. Studies have identified non-spherical Pt nanoparticles on carbon supports as promising approaches to address this challenge. However, to realize the full benefits of these strategies, the catalyst synthesis procedures must be successfully simplified and scaled up, and the catalyst must perform well in half and full-cell tests. In this study, a surfactant-free one-pot method is developed to synthesize non-spherical Pt nanoparticles on Ketjen Black carbon, which is either non-treated (Pt/KB), acid-treated (Pt/KB-O), or nitrogen-doped (Pt/KB-N). The catalysts are synthesized in both small and large batches to determine the effect of scaling up the synthesis procedure. The nitrogen-doped carbon support shows a nearly identical morphological structure with uniform distribution of non-spherical Pt nanoparticles for both small and large batches' synthesis compared with non-treated and acid-treated carbon samples. The comparative oxygen reduction reaction (ORR) activity shows that the Pt/KB-N prepared in small and large batches has better ORR activity, which is likely caused by uniformly distributed non-spherical Pt nanoparticles on the nitrogen-doped carbon support. All three catalysts show similar ORR durability, testing from 0.5–1.0 V, while Pt/KB-O displays slightly better durability from 1.0–1.5 V for carbon corrosion. These results will help inform the implementation of shape-controlled Pt catalysts on modified carbon supports in large scale.

Keywords: shape-controlled catalysts; carbon support; nitrogen doping; one-pot synthesis; ORR activity; accelerated stress tests



check for updates

Citation: Lim, M.; Khalid, M.; Shahgaldi, S.; Li, X. Development of Non-Spherical Platinum Nanoparticles on Carbon Supports for Oxygen Reduction Reaction. *Catalysts* **2023**, *13*, 1322. <https://doi.org/10.3390/catal13101322>

Academic Editors: Menggang Li, Shuo Geng and Manyi Gao

Received: 30 August 2023

Revised: 18 September 2023

Accepted: 18 September 2023

Published: 25 September 2023



Copyright: © 2023 by the authors. Licensee MDPI, Basel, Switzerland. This article is an open access article distributed under the terms and conditions of the Creative Commons Attribution (CC BY) license (<https://creativecommons.org/licenses/by/4.0/>).

1. Introduction

Proton exchange membrane (PEM) fuel cells operating on green hydrogen are anticipated to play an important role in decarbonizing the global energy system, with hydrogen anticipated to contribute up to 18–24% of final energy demands by the middle of this century [1,2]. They convert the chemical energy of the reactants (most often H₂ and O₂) directly into electrical energy, thereby enabling efficient and zero-emission energy conversion and power generation. PEM fuel cells are recognized as emerging clean power and propulsion systems for sustainable aviation [3], passenger vehicles, and heavy-duty transportation [4–6], sectors that are most difficult to decarbonize with conventional energy conversion technologies, and they are ideally suited to complement batteries in electric vehicles [5]. Despite tremendous progress in the last few decades, PEM fuel cell systems remain too expensive for widespread adoption as energy conversion devices, with a substantial portion of their cost coming from platinum (Pt)-based catalysts [7]. Therefore, the Pt loading must be reduced to make them more economical. This reduction in Pt loading is accomplished by improving the performance of the catalyst used, specifically for the

oxygen reduction reaction (ORR), and optimizing the fuel cell electrodes to maximize catalyst utilization.

Shape-controlled Pt nanostructures have potential to improve the activity and durability of Pt in electrocatalytic applications. The quasi-spherical morphology of commercially available Pt nanoparticle (NP) catalysts is suboptimal because its area-to-volume ratio and intrinsic activity are lower than those of non-spherical structures [8,9]. Therefore, shape control can potentially increase the electrochemically active surface area (ECSA), specific activity (SA), and mass activity (MA) of the electrocatalyst. Shape-controlled structures realize specific crystal facets (e.g., (100), (111), and (110)) on the nanoscale, altering the catalyst's chemical and electronic interactions and leading to controllable catalytic selectivity and improved performance [10]. Examples of shape-controlled NP morphologies that have been studied include cubes [11,12], octahedra [13], tetrahedra [14], and more complex shapes with high-index facets [15]. In addition to close-packed NPs, one- and two-dimensional structures such as nanowires have been characterized [16]. Many of these studies report benefits such as high ORR activity, good durability against voltage cycling, and preferential CO oxidation. Because of such promising properties, shape-controlled Pt and Pt-alloy catalysts are being considered in actual PEM fuel cells [17–20].

To further improve its dispersion, stability, and electronic conductivity, as well as to form sufficiently large pore structures for reactant mass transport, Pt is often deposited on a much larger carbon substrate, creating a carbon-supported Pt catalyst (Pt/C). The carbon support is a crucial component of the catalyst layer (CL) in a membrane-electrode assembly (MEA). Most commercially available fuel cell catalysts employ carbon blacks (e.g., Vulcan carbon and Ketjen Black) as the support [5], but graphitized carbon materials such as carbon nanotubes, reduced graphene oxide, graphene nanoplates, and graphite nanofibers can also be used [21]. Experimental studies show that the choice of carbon material impacts both the activity and durability of the catalyst [22,23]. Furthermore, carbon can be functionalized using methods such as oxidizing acid treatment [24–26] and nitrogen (or other heteroatom) doping [5,27,28] to introduce surface groups that serve as nucleation sites for Pt NPs. These functionalization methods are known to impact the carbon's surface chemistry and microstructure. For example, oxidation treatment introduces carboxyl groups onto the surface, increasing its hydrophilicity [29], electronegativity [30], and adhesion force on Pt [31], while degrading the carbon's porous structure and surface area [26]. Meanwhile, nitrogen doping alters the electronic interaction between Pt and carbon [30], and it may affect the carbon's surface area and hydrophilicity depending on what kind of carbon is used [32].

Although many experimental and theoretical studies have verified the benefits of Pt shape control and carbon support functionalization, few studies have addressed large-scale production of advanced catalysts that use these strategies. Many catalysts reported in the literature use samples no larger than a few dozen milligrams, which is insufficient for commercial applications [33–36]. The synthesis of Pt/C can be difficult to simplify and scale up without affecting the catalyst's properties [33], especially for shape-controlled catalysts, which are often synthesized using shape-controlling agents that need to be removed from the catalyst surface [10]. Therefore, it would be advantageous to synthesize these catalysts using methods that are easily scalable and avoid difficult-to-remove shape-controlling agents.

Furthermore, the synthesis of shape-controlled catalysts in large quantities requires careful control of conditions for the synthesis process, so shape-controlled Pt/C catalysts are typically synthesized in two steps. The first step is to synthesize the shape-controlled Pt NPs, and the second is to deposit the synthesized Pt NPs on the functionalized carbon support [37]. In addition to increasing production costs for commercial applications, the process of physically mixing Pt NPs and carbon may fail to bond the NPs strongly to the carbon, adversely affecting the catalyst's stability [37]. Substituting this process with a one-pot synthesis method, wherein the Pt/C catalyst is formed directly from the Pt precursor and carbon support, would be preferable. However, accurately controlling the

Pt NP morphology using one-pot methods can be difficult; this is further complicated when using functionalized carbon supports, as the surface chemistry affects the interaction between the Pt precursor and carbon, changing the NP size and dispersion [38]. One-pot synthesis of shape-controlled and carbon-supported Pt catalysts must be improved before such catalysts can be deployed in large scale.

Finally, the good performance of advanced electrocatalysts in ex situ electrochemical tests does not always translate into good performance in actual PEM fuel cells. The full potential of these catalysts can only be unleashed when paired with an optimal CL structure, which can efficiently transport gaseous reactants, liquid water, and ions to and from the catalyst. CL optimization is recognized as an important research area for shape-controlled Pt-based catalysts [9]. Carbon functionalization can play a role in improving PEM fuel cell performance because the carbon support is an integral component of the CL. For example, nitrogen groups in the carbon may promote a more uniform distribution of ionomer on the catalyst surface [32,39], thereby minimizing oxygen and proton transport resistances in the cathode CL. To date, few studies have tested shape-controlled catalysts with treated carbon supports in a manner representative of practical applications, with aspects such as scaled-up catalyst synthesis and MEA testing.

Therefore, the objectives of this study are to: (i) synthesize shape-controlled and carbon-supported Pt catalysts in one step, using what is often referred to as one-pot synthesis; and (ii) evaluate the effects of carbon support on the non-spherical Pt catalyst, followed by a comparison of its performance when synthesized in both small and large batches. The as-developed catalysts are characterized physically and electrochemically for their performance and stability. Rather than simply aiming for the highest ECSA and SA values based on electrochemical tests, the catalyst is developed in a manner suitable for mass production and application in MEAs. The selected catalyst synthesis method is a one-pot and surfactant-free solvothermal method that has previously been used to produce various non-spherical Pt nanostructure catalysts [40]. To determine how well it scales up, the catalyst synthesis is conducted in both small batches (a few dozen mg Pt) and large batches (a few hundred mg Pt), with the latter corresponding to the size used in our previous work [41].

2. Experimental Section

2.1. Materials and Chemicals

Ketjen Black EC-600JD carbon powder (AkzoNobel), hydrochloric acid (37%, Sigma-Aldrich, St. Louis, MO, USA), sulfuric acid (95–98%, Sigma-Aldrich), nitric acid (70%, Caledon Laboratories, Georgetown, ON, Canada), chloroplatinic acid hexahydrate ($\geq 37.50\%$ Pt basis, Sigma-Aldrich), ethylene glycol (Fisher Scientific), N,N-dimethylformamide ($\geq 99.8\%$, Sigma-Aldrich), sodium hydroxide ($\geq 97.0\%$, Sigma-Aldrich), ethanol (HPLC, Sigma-Aldrich), Nafion (5% solution, Ion Power, New Castle, DE, USA), and perchloric acid (70%, GFS Chemicals, Powell, OH, USA) are used as received. Nitrogen (99.998%), argon (99.998%), and oxygen (99.993%) compressed gas cylinders are obtained from Linde. Deionized water is supplied from our laboratory.

2.2. Carbon Treatment

All of the carbon supports used in this work are derived from Ketjen Black EC-600JD carbon. Non-treated, oxidized, and nitrogen-doped carbon are denoted by KB, KB-O, and KB-N, respectively (Figure 1). To prepare KB, 6 g of the carbon material is mixed with 800 mL of 2.5 M hydrochloric acid and then refluxed at 120 °C for 18 h. After cooling overnight, the carbon is collected and heated again in 800 mL of deionized water (DIW) at 120 °C for 8 h. The carbon is washed 3–4 times using DIW until it is approximately pH-neutral and dried inside a temperature-controlled chamber at 85 °C to obtain the final product. To prepare KB-O, 2 g of KB is mixed with 67 mL of 4 M sulfuric acid and 200 mL of 4 M nitric acid and then refluxed at 120 °C for 4 h. The carbon is washed and dried as described above to obtain the final product. To prepare KB-N, 1.6 g of KB is dispersed

in 100 mL of DIW, and 5 g dicyanamide is dissolved in 40 mL of hot DIW. After stirring these together for 30 min, the mixture is heated at 180 °C for 20 h in an autoclave and then washed repeatedly with DIW. Following this, the carbon is mixed into 75 mL ammonium hydroxide and similarly heated at 180 °C for 20 h. Finally, the carbon is treated with N₂ gas at 900 °C to obtain the final product.

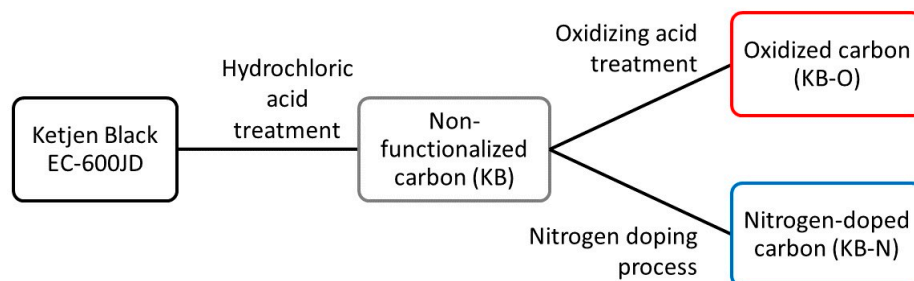


Figure 1. Summary of the three carbon supports prepared in this study.

2.3. Catalyst Synthesis

Non-spherical Pt NPs supported on carbon are synthesized using a modified one-pot solvothermal synthesis method similar to those reported in previous studies [14,16,42]. In a typical synthesis, 600 mg of sodium hydroxide is dissolved in 8 mL of ethylene glycol (EG) and 12 mL of N,N-dimethylformamide (DMF). Following that, 100 mg of H₂PtCl₆·6H₂O is added to the flask, and the mixture sonicated for 20 min; then, 40 mg of carbon (KB, KB-O, or KB-N) is added, and the mixture is sonicated for another 20 min. After stirring overnight, the mixture is heated at 170 °C for 8 h under an N₂ atmosphere, followed by natural cooling to room temperature. The catalyst is washed 3–4 times using DIW and ethanol, followed by drying in air for 48 h and inside a temperature-controlled chamber at 70 °C for 24 h. This synthesis procedure yields a nominal Pt content of 48.5 wt.%. To synthesize the catalyst in large batches, the procedure is repeated with all reactant quantities scaled up tenfold (i.e., using 1 g of H₂PtCl₆·6H₂O).

In this study, the catalyst names indicate which carbon support they contain (KB, KB-O, or KB-N) and whether they are synthesized at small or large scale (1× or 10×). The small-scale catalyst samples on KB, KB-O, and KB-N are called Pt/KB, Pt/KB-O, and Pt/KB-N, respectively; the corresponding large-scale samples are referred to as Pt/KB-10×, Pt/KB-O-10×, and Pt/KB-N-10×, respectively.

2.4. Physical Characterization

Physical characterization techniques are used to compare the surface chemistry and microstructure of the treated carbon supports. Brunauer–Emmett–Teller (BET) area measurements are taken using a Micromeritics Gemini VII 2390a machine with N₂ as the adsorbate. To calculate the area, the BET equation is applied to the region where P/P_0 is approximately 0.05–0.30, and the cross-sectional area of one adsorbate molecule is taken as 0.162 nm² [43]. X-ray photoelectron spectroscopy (XPS) measurements are taken using a VGS ESCALab 250 Imaging ESCA system with Al K α radiation (1486.68 eV).

Transmission electron microscopy (TEM) images of the catalyst samples are captured using a Zeiss Libra 200 MC system operating at 200 kV, with images taken at a range of magnification values (50 k×, 100 k×, 200 k×, and 400 k×). NP size distributions are estimated by manually measuring 200–300 particles from at least two different 200 k× images. Powder X-ray diffraction (XRD) measurements are taken using Rigaku Miniflex II and Bruker D8 machines to characterize the crystallographic structures of the three large-scale samples. A full scan is taken between $2\theta = 20\text{--}90^\circ$, followed by a detailed scan of the Pt(111) peak to provide a second estimate of the crystallite size (with the Scherrer constant taken as 0.9). Thermogravimetric analysis (TGA) measurements are taken using a TA Instruments TGA Q500 machine to estimate the mass fractions of Pt. Approximately

7–10 mg of each catalyst sample is heated in air between room temperature and 700–750 °C to oxidize the carbon support, thus revealing the mass of Pt remaining in the sample.

2.5. Electrochemical Characterization

The ORR performance of the catalysts is determined by half-cell (ex situ) electrochemical characterization. Tests are conducted using a BAS RRDE-3A system and a CH Instruments 760E potentiostat. For each test, 5 mg (± 0.2 mg) of the catalyst sample is dispersed in 0.5 mL DIW, 4.5 mL ethanol, and 30 μ L 5% Nafion solution and sonicated for 25–30 min to form a homogeneous catalyst ink. Then, 6.4 μ L of this ink is cast onto a glassy carbon electrode (4 mm diameter) and dried in air to form the working electrode. A reversible hydrogen electrode (RHE) is used as the reference electrode, a Pt wire as the counter electrode, and 0.1 M perchloric acid as the electrolyte. All tests are conducted at room temperature (around 21.5 °C). To ensure repeatability of the results, each catalyst sample is tested multiple times with at least 3 different inks.

Cyclic voltammetry (CV) measurements are taken by running 50 cycles between 0.05 and 1.2 V (vs. RHE) at 0.5 V/s to activate the catalyst, followed by 5 cycles at 0.1 V/s to collect the actual data. The catalyst's ECSA is calculated using the H₂ desorption peak area. Linear sweep voltammetry (LSV) measurements are taken from 0.1–1.2 V (vs. RHE) in the positive direction with a scan rate of 0.02 V/s, with rotation speeds of 800, 1200, 1600, 2000, and 2400 rpm. Background noise correction is accomplished by taking the difference between measurements in N₂- and O₂-saturated electrolyte. The catalyst's MA and SA are calculated based on the 1600 rpm data at 0.9 V (vs. RHE), consistent with U.S. Department of Energy standards [44]. Two additional tests are run to study the catalyst's durability against potential cycling. A catalyst accelerated stress test (AST) is performed by cycling 20,000 times between 0.5 and 1 V (vs. RHE) using a scan rate of 0.5 V/s to repeatedly oxidize and reduce the catalyst surface [44]. Similarly, a carbon corrosion AST is performed by cycling 5000 times between 1 and 1.5 V (vs. RHE) to simulate the effects of unmitigated fuel cell startups and shutdowns [44].

3. Results and Discussion

3.1. Carbon Support Properties

From BET area measurement, the surface areas of KB, KB-O, and KB-N are estimated to be 1101, 924, and 1305 m²/g, respectively (Figure S1, Supporting Information). These discrepancies suggest that the chemical treatment of Ketjen Black carbon affects its physical properties, which in turn could affect the deposition of Pt NPs during one-pot catalyst synthesis. For KB-O, the loss of BET area confirms the previous results in the literature [26]. For KB-N, the increase in BET area could be explained by an etching and opening of the Ketjen Black carbon's porous structure, similar to a previous study also using Ketjen Black [39].

Judging from the XPS survey measurements (Figure S2a, Supporting Information), all three carbon powders exhibit clear peaks at the binding energies corresponding to C 1s (284–285 eV) and O 1s (532–534 eV). The O 1s peak has the highest relative intensity for KB-O, confirming the effectiveness of oxidation treatment on this sample. Figure S2b (Supporting Information) shows an enlarged scan between 397 and 404 eV, where a highest-intensity peak around 398–399 eV indicates the successful doping of nitrogen in the carbon network [45–47]. Meanwhile, KB-O exhibits two peaks, with the stronger one (405–408 eV) corresponding to nitrogen oxides and the weaker one (398–403 eV) possibly corresponding to quaternary and pyrrolic N; these signals indicate residue from nitric acid treatment [30].

3.2. Catalyst Properties

Figure 2a,c,e show representative TEM images captured at 200 k \times magnification for the three small-scale catalyst samples. Pt/KB is composed of small NPs (approx. 2 nm diameter) along with some larger NPs or agglomerates (≥ 8 nm). In contrast, Pt/KB-O and Pt/KB-N are characterized by mixtures of medium-sized NPs (approx. 5 nm) and small

NPs. Based on the 200 k \times magnification images, the mean NP sizes for Pt/KB, Pt/KBO, and Pt/KB-N are 2.1, 3.2, and 2.4 nm, respectively (Figure 3a,c,e). The differences between Pt/KB, Pt/KB-O, and Pt/KB-N can be explained by differences in the modified carbon's surface chemistry and microstructure. For example, the medium-sized NPs in Pt/KB-O and Pt/KB-N appear to be dispersed better compared to the large agglomerates in Pt/KB, and this can be explained by the functional groups on KB-O and KB-N, which serve as binding sites for the NPs. Furthermore, Pt/KB-O has a larger average NP size than Pt/KB and Pt/KB-N, which can be explained by the lower BET surface area of KB-O, as well as its electronegativity (which makes it difficult for the negatively charged Pt precursor, PtCl₆²⁻, to nucleate into small NPs). Overall, the TEM images suggest that surface groups on both KB-O and KB-N improve the dispersion of NPs on the support, which should theoretically benefit the catalyst because of increased ECSA.

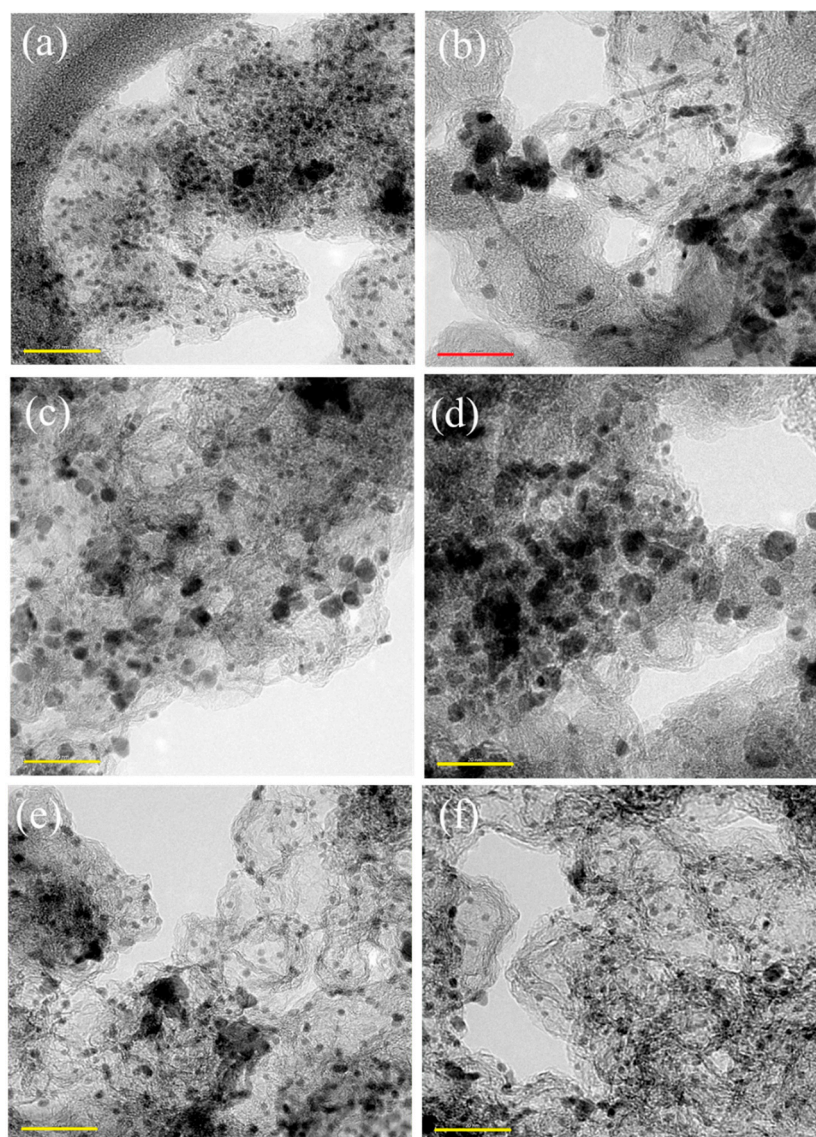


Figure 2. TEM images of (a) Pt/KB, (b) Pt/KB-10 \times , (c) Pt/KB-O, (d) Pt/KB-O-10 \times , (e) Pt/KB-N, and (f) Pt/KB-N-10 \times captured at 200 k \times magnification. The scale bars are 20 nm.

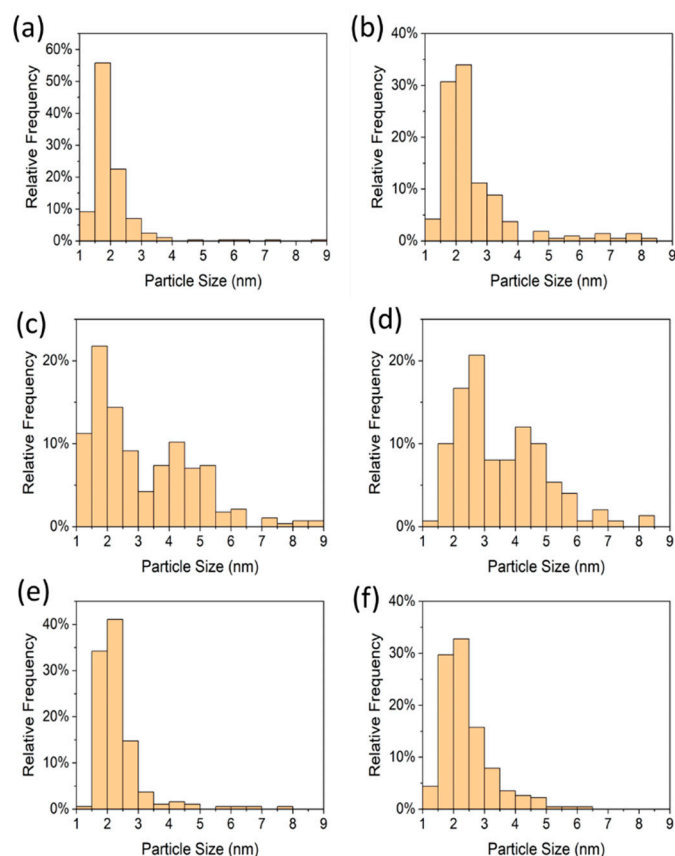


Figure 3. Particle size distributions for (a) Pt/KB, (b) Pt/KB-10 \times , (c) Pt/KB-O, (d) Pt/KB-O-10 \times , (e) Pt/KB-N, and (f) Pt/KB-N-10 \times . Note that the size distribution for Pt/KB-10 \times excludes the nanorods.

Figure 2b,d,f show representative TEM images captured at 200 k \times magnification for the three large-scale catalyst samples. Unlike Pt/KB-10 \times and Pt/KB-O-10 \times , the morphological structure of Pt/KB-N-10 \times is visually more similar to its small-scale version, without obvious agglomeration of Pt nanoparticles [48]. This result suggests that the nitrogen-doped carbon support may promote a more consistent or predictable catalyst morphology when the catalyst synthesis is scaled up. Compared to the small batches, the mean NP sizes increase for Pt/KB-10 \times and Pt/KB-O-10 \times (2.6 and 3.5 nm, respectively), whereas Pt/KB-N-10 \times maintains a similar size (2.4 nm).

Figure 4 shows the XRD patterns of Pt/KB-10 \times , Pt/KB-O-10 \times , and Pt/KB-N-10 \times . All the samples display clear peaks corresponding to Pt(111), Pt(200), Pt(220), Pt(311), and Pt(222), confirming the crystalline structure of the Pt catalyst. The peak locations and relative intensities are similar to those measured on commercial Pt/C catalysts [49]. In addition, the Pt(111) peak of each sample is scanned at a slower rate to measure peak broadening, based on which the crystallite sizes are estimated to be 5.8, 5.6, and 5.6 nm, respectively. These values are noticeably larger than the mean sizes determined from TEM. A plausible explanation is that the samples contain many small NPs, which result in a small mean size according to TEM, but the small NPs also have very small volume, so their large quantity does not accurately represent the actual distribution of Pt atoms. In reality, many Pt atoms are located within the few large NPs and agglomerates, which is probably what is being captured by the XRD results.

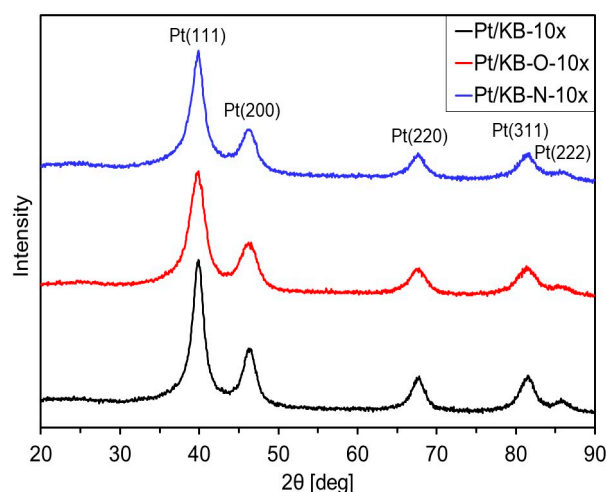


Figure 4. XRD patterns for Pt/KB-10 \times , Pt/KB-O-10 \times , and Pt/KB-N-10 \times .

Judging from the TGA measurement, the Pt loadings for all catalysts except Pt/KB-N-10 \times are estimated to be from 47–52 wt.%, close to the nominal Pt loading of 48.5 wt.% (Figure S3, Supporting Information). This confirms that most of the Pt precursor is successfully reduced and deposited onto the carbon support. Meanwhile, the Pt loading for Pt/KB-N-10 \times is slightly lower at 43 wt.%, which may be due to experimental factors during the TGA measurement. Furthermore, the different catalyst samples are observed to lose mass from carbon oxidation at different temperatures, with Pt/KB-O-10 \times losing mass at a lower temperature and Pt/KB-N-10 \times at a higher temperature compared to Pt/KB-10 \times , despite all catalysts having similar Pt loadings. This observation shows that KB-O is less thermally stable and KB-N more thermally stable than KB.

3.3. Electrochemical Performance

Figure 5a compares the average CV curves obtained for Pt/KB, Pt/KB-O, Pt/KB-N, and commercial Pt/C. Based on the hydrogen desorption peak area (measured using the baseline at 0.4 V), the ECSA values for these catalysts are calculated as 25, 31, 25, and 45.47 m²/g, respectively. Despite having a more uniform Pt nanoparticle distribution on the carbon network, Pt/KB-N displayed a relatively smaller ECSA, which might be due to a thicker carbon surface surrounding the Pt nanoparticles. Additionally, the widened middle parts of the CV curves (approx. 0.4–0.6 V) for the as-synthesized catalysts represent higher double-layer capacitance compared with commercial Pt/C, which may increase their accessibility to the aqueous electrolyte [50]. Interestingly, when the synthesis is scaled up, Pt/KB-N-10 \times shows a relatively larger ECSA (31 m²/g) compared to Pt/KB-10 \times and Pt/KB-O-10 \times (24 and 25 m²/g, respectively) (Figure S4, Supporting Information). This may be because Pt/KB-N-10 \times retains a large quantity of Pt nanoparticles, and their uniform distribution is without obvious agglomeration, according to the TEM analysis.

The ORR activity of the as-synthesized catalysts was studied using RDE in oxygen-saturated 0.1 M HClO₄. Figure 5b compares the average LSV curves for Pt/KB, Pt/KB-O, Pt/KB-N, and commercial Pt/C. The mass activity (MA) values towards the ORR at 0.9 V (vs. RHE) for these catalysts are 101, 103, 115, and 126.4 A/g, respectively. Combined with the ECSA measurements corresponding to the LSV tests, the specific activity (SA) values are 4.1, 3.2, 4.7, and 2.7 A/m², respectively. Among the as-synthesized catalysts, Pt/KB-N achieves the highest MA of 115 A/g, but this is slightly lower than that of commercial Pt/C. However, its SA outcompetes commercial Pt/C, at 4.7 A/m². This is likely caused by the uniform distribution of Pt nanoparticles on the nitrogen-doped carbon surface compared to non-treated and acid-treated samples [51]. Furthermore, we measured the LSV curves for large-batch samples (Pt/KB-10 \times , Pt/KB-O-10 \times , and Pt/KB-N-10 \times) and compared them with Pt/KB, Pt/KB-O, and Pt/KB-N, as shown in Figure 5c. The MA values towards

the ORR of these catalysts are 141, 114, and 148 A/g, corresponding to SA values of 5.7, 4.7, and 4.9 A/m², respectively. All samples show enhanced ORR activity upon scaleup. However, Pt/KB-10 \times displayed a significant improvement in both MA and SA compared to Pt/KB-O and Pt/KB-N. This result suggests that carbon support modification with small- and large-batch synthesis does not always replicate the catalytic activity of the catalysts.

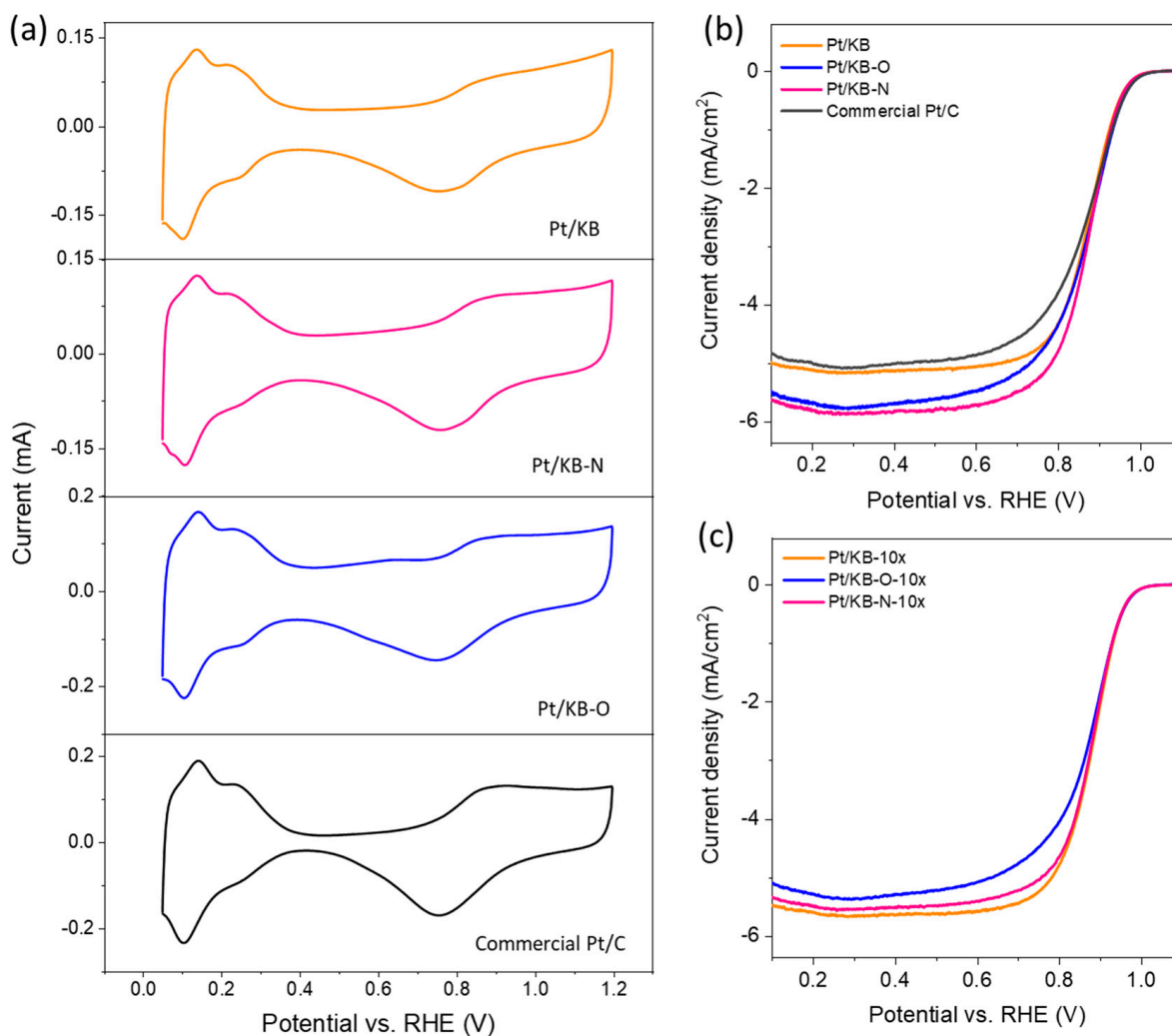


Figure 5. Cyclic voltammetry curves measured in nitrogen-saturated 0.1 M HClO₄ electrolyte for (a) Pt/KB, Pt/KB-O, Pt/KB-N; and linear sweep voltammograms measured in oxygen-saturated 0.1 M HClO₄ electrolyte for (b) Pt/KB, Pt/KB-O, Pt/KB-N, and (c) Pt/KB-10 \times , Pt/KB-O-10 \times , Pt/KB-N-10 \times .

Figure 6 summarizes the changes in ECSA during AST between 0.5 and 1 V (vs. RHE). Pt/KB loses approximately 17% of its initial ECSA after 20,000 potential cycles, whereas Pt/KB-O and Pt/KB-N lose 23% and 24%, respectively. The losses in ECSA for all the large-scale samples are between 22 and 24%. Based on these results, substituting KB with KB-O or KB-N does not necessarily increase the durability of the supported Pt catalyst. For catalysts on porous high-surface-area carbon supports, such as Ketjen Black, the electrochemical degradation is thought to be dominated by Ostwald ripening [23]. Therefore, it is reasonable to conclude that the chemically treated carbon supports do little to prevent the Pt NPs from degrading via Ostwald ripening.

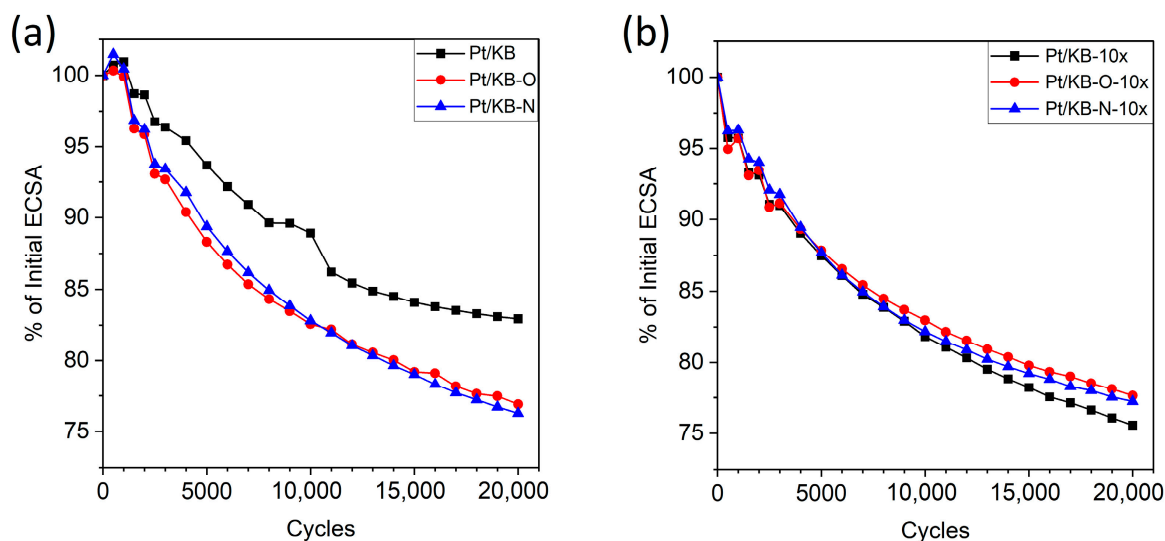


Figure 6. Comparison of ECSA degradation rates during the catalyst AST for (a) Pt/KB, Pt/KB-O, Pt/KB-N; and (b) Pt/KB-10 \times , Pt/KB-O-10 \times , Pt/KB-N-10 \times .

Figure 7 summarizes the changes in ECSA during the corrosion AST from 1–1.5 V (vs. RHE). In this test, Pt/KB, Pt/KB-O, and Pt/KB-N lose 18%, 4%, and 12%, respectively, of their initial ECSA after 5000 cycles. The large-scale catalysts show a similar trend, with Pt/KB-10 \times , Pt/KB-O-10 \times , and Pt/KB-N-10 \times losing 17%, 7%, and 21%, respectively. The Pt catalysts on KB-O are the most resistant against ECSA loss, seemingly contradicting other studies on carbon corrosion [50], but there are some possible explanations for this result. First, unlike the catalyst AST, the corrosion AST is expected to cause some Pt particle detachment [52]. Because Pt/KB-O and Pt/KB-O-10 \times have fewer small NPs (which are more thermodynamically unstable) and possibly stronger adhesion between Pt and the surface [31], these catalysts may be more resistant to Pt detachment. Second, KB and KB-N seem to gain more new oxygen-containing groups (carboxyl, carbonyl, etc.) on the surface, signaling the corrosion and poisoning of the Pt catalyst [53]. It is possible that existing oxygen groups formed on KB-O during the oxidation treatment protect the surface from further corrosion. Thus, chemically treated carbon may indirectly affect the durability of a Pt catalyst in high-voltage or corrosive conditions by limiting the effects of particle detachment or newly formed oxygen-containing groups. However, this discussion is speculative and cannot determine which mechanism is most responsible for the ECSA loss.

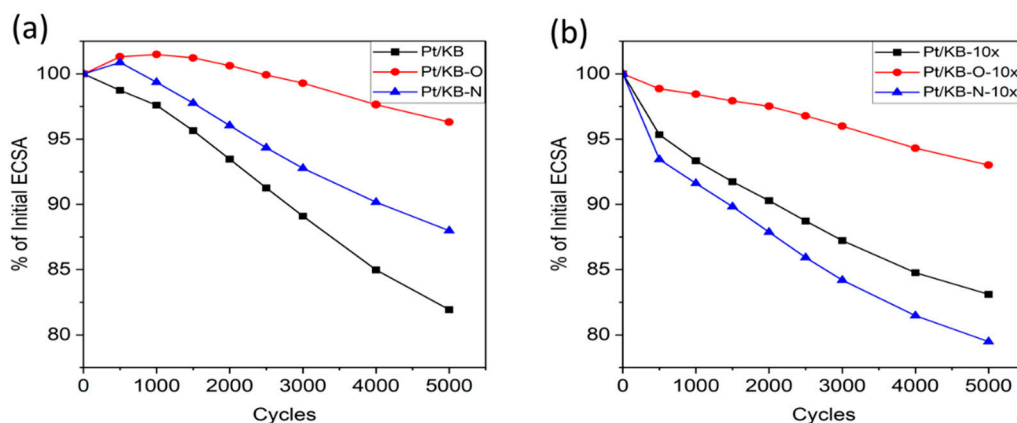


Figure 7. Comparison of ECSA degradation rates during the carbon corrosion AST for (a) Pt/KB, Pt/KB-O, Pt/KB-N; and (b) Pt/KB-10 \times , Pt/KB-O-10 \times , Pt/KB-N-10 \times .

All the results related to this study, including TEM images at different resolutions and CVs before and after durability tests, are available elsewhere [48].

4. Conclusions

In this study, a surfactant-free one-pot method is developed to synthesize non-spherical Pt catalysts on chemically treated carbon supports in both small and large batches. It is found that chemically treating Ketjen Black carbon (KB) with oxidizing acids (KB-O) or a nitrogen doping process (KB-N) affects its surface chemistry and microstructure, which in turn impact the properties of the supported Pt catalyst. For Pt/KB-O, the oxidation treatment adds binding sites to KB-O, ensuring the formation of individual nanoparticles (NPs), but the reduced BET area and modified surface chemistry lead to a larger mean NP size. Meanwhile, for Pt/KB-N, nitrogen doping also adds binding sites to KB-N while increasing its BET area, also leading to well-dispersed NPs. Both functionalization methods lead to more predictable morphology when the catalyst synthesis procedure is scaled up. Electrochemical characterization indicates that Pt/KB-O has similar or slightly lower oxygen reduction reaction (ORR) activity, and Pt/KB-N similar or slightly higher activity, compared to Pt/KB. From the accelerated stress tests, neither Pt/KB-O nor Pt/KB-N is more durable than Pt/KB when cycled between 0.5 and 1.0 V, but Pt/KB-O is more durable than Pt/KB when cycled between 1.0 and 1.5 V. Overall, this study shows that chemical treatment of the carbon support can improve a Pt catalyst's dispersion, but the effects on ORR activity and durability are highly complex and depend on a multitude of factors. The results presented here can inform future studies on non-spherical Pt-based catalysts, chemically modified carbon supports, or both these topics.

Supplementary Materials: The following supporting information can be downloaded at: <https://www.mdpi.com/article/10.3390/catal13101322/s1>, Figure S1: Plot for BET surface area; Figure S2: XPS survey spectra; Figure S3: TGA plot for the samples; Figure S4: CV curves for the as-synthesized samples.

Author Contributions: M.L.: Investigation; methodology; formal analysis; visualization; writing—original draft; M.K.: Draft preparation; writing—reviewing, editing; formal analysis; visualization; S.S.: Methodology, validation, Co-supervision; X.L. Conceptualization, Funding acquisition, methodology, Project administration, Resources, Supervision. All authors have read and agreed to the published version of the manuscript.

Funding: This work received financial support from the Canadian Urban Transit Research and Innovation Consortium (CUTRIC) via Project Number 160028, Ballard Power Systems Inc. via SRA#077701, and the Natural Sciences and Engineering Research Council of Canada (NSERC) via a CRD Grant (CRDPJ 522410-17) and a Discovery Grant. Ballard not only funded but also gave some insights into the analysis.

Data Availability Statement: Not applicable.

Conflicts of Interest: There is no conflict of interest associated with this manuscript.

References

1. International Renewable Energy Agency. Global Energy Transformation: A Roadmap to 2050 (2019 Edition). 2019. Available online: https://www.irena.org/-/media/Files/IRENA/Agency/Publication/2019/Apr/IRENA_Global_Energy_Transformation_2019.pdf (accessed on 13 March 2023).
2. Natural Resources Canada. Hydrogen Strategy for Canada (Seizing the Opportunities for Hydrogen). 2020. Available online: https://natural-resources.canada.ca/sites/nrcan/files/environment/hydrogen/NRCan_Hydrogen-Strategy-Canada-na-en-v3.pdf (accessed on 13 March 2023).
3. Baroutaji, A.; Wilberforce, T.; Ramadan, M.; Olabi, A.G. Comprehensive investigation on hydrogen and fuel cell technology in the aviation and aerospace sectors. *Renew. Sustain. Energy Rev.* **2019**, *106*, 31–40. [CrossRef]
4. Banham, D.; Ye, S. Current Status and Future Development of Catalyst Materials and Catalyst Layers for Proton Exchange Membrane Fuel Cells: An Industrial Perspective. *ACS Energy Lett.* **2017**, *2*, 629–638. [CrossRef]
5. Banham, D.; Zou, J.; Mukerjee, S.; Liu, Z.; Yang, D.; Zhang, Y.; Peng, Y.; Dong, A. Ultralow platinum loading proton exchange membrane fuel cells: Performance losses and solutions. *J. Power Sources* **2021**, *490*, 229515. [CrossRef]

6. Cullen, D.A.; Neyerlin, K.C.; Ahluwalia, R.K.; Mukundan, R.; More, K.L.; Borup, R.L.; Weber, A.Z.; Myers, D.J.; Kusoglu, A. New roads and challenges for fuel cells in heavy-duty transportation. *Nat. Energy* **2021**, *6*, 462–474. [[CrossRef](#)]
7. Wang, X.X.; Swihart, M.T.; Wu, G. Achievements, challenges and perspectives on cathode catalysts in proton exchange membrane fuel cells for transportation. *Nat. Catal.* **2019**, *2*, 578–589. [[CrossRef](#)]
8. Mahata, A.; Nair, A.S.; Pathak, B. Recent advancements in Pt-nanostructure-based electrocatalysts for the oxygen reduction reaction. *Catal. Sci. Technol.* **2019**, *9*, 4835–4863. [[CrossRef](#)]
9. Wang, Y.-J.; Long, W.; Wang, L.; Yuan, R.; Ignaszak, A.; Fang, B.; Wilkinson, D.P. Unlocking the door to highly active ORR catalysts for PEMFC applications: Polyhedron-engineered Pt-based nanocrystals. *Energy Environ. Sci.* **2018**, *11*, 258–275. [[CrossRef](#)]
10. Leong, G.J.; Schulze, M.C.; Strand, M.B.; Maloney, D.; Frisco, S.L.; Dinh, H.N.; Pivovar, B.; Richards, R.M. Shape-directed platinum nanoparticle synthesis: Nanoscale design of novel catalysts. *Appl. Organomet. Chem.* **2014**, *28*, 1–17. [[CrossRef](#)]
11. Li, F.; Gao, X.; Xue, Q.; Li, S.; Chen, Y.; Lee, J.-M. Reduced graphene oxide supported platinum nanocubes composites: One-pot hydrothermal synthesis and enhanced catalytic activity. *Nanotechnology* **2015**, *26*, 65603. [[CrossRef](#)]
12. Moghaddam, R.B.; Shahgaldi, S.; Li, X. A facile synthesis of high activity cube-like Pt/carbon composites for fuel cell application. *Front. Energy* **2017**, *11*, 245–253. [[CrossRef](#)]
13. Sánchez-Sánchez, C.M.; Solla-Gullón, J.; Vidal-Iglesias, F.J.; Aldaz, A.; Montiel, V.; Herrero, E. Imaging Structure Sensitive Catalysis on Different Shape-Controlled Platinum Nanoparticles. *J. Am. Chem. Soc.* **2010**, *132*, 5622–5624. [[CrossRef](#)] [[PubMed](#)]
14. Rana, M.; Chhetri, M.; Loukya, B.; Patil, P.K.; Datta, R.; Gautam, U.K. High-Yield Synthesis of Sub-10 nm Pt Nanotetrahedra with Bare 111 Facets for Efficient Electrocatalytic Applications. *ACS Appl. Mater. Interfaces* **2015**, *7*, 4998–5005. [[CrossRef](#)]
15. Wu, R.; Tsiakaras, P.; Shen, P.K. Facile synthesis of bimetallic Pt-Pd symmetry-broken concave nanocubes and their enhanced activity toward oxygen reduction reaction. *Appl. Catal. B Environ.* **2019**, *251*, 49–56. [[CrossRef](#)]
16. Hoque, M.A.; Hassan, F.M.; Jauhar, A.M.; Jiang, G.; Pritzker, M.; Choi, J.-Y.; Knights, S.; Ye, S.; Chen, Z. Web-like 3D Architecture of Pt Nanowires and Sulfur-Doped Carbon Nanotube with Superior Electrocatalytic Performance. *ACS Sustain. Chem. Eng.* **2018**, *6*, 93–98. [[CrossRef](#)]
17. Sakamoto, R.; Omichi, K.; Furuta, T.; Ichikawa, M. Effect of high oxygen reduction reaction activity of octahedral PtNi nanoparticle electrocatalysts on proton exchange membrane fuel cell performance. *J. Power Sources* **2014**, *269*, 117–123. [[CrossRef](#)]
18. Li, B.; Wang, J.; Gao, X.; Qin, C.; Yang, D.; Lv, H.; Xiao, Q.; Zhang, C. High performance octahedral PtNi/C catalysts investigated from rotating disk electrode to membrane electrode assembly. *Nano Res.* **2019**, *12*, 281–287. [[CrossRef](#)]
19. Kim, C.; Lee, H. Applying Shape-Controlled Pt Nano-dendrites Supported on Carbon for Membrane-Electrode Assembly in a Proton Exchange Membrane Fuel Cell. *Fuel Cells* **2013**, *13*, 889–894. [[CrossRef](#)]
20. Fang, B.; Daniel, L.; Bonakdarpour, A.; Govindarajan, R.; Sharman, J.; Wilkinson, D.P. Dense Pt Nanowire Electrocatalyst for Improved Fuel Cell Performance Using a Graphitic Carbon Nitride-Decorated Hierarchical Nanocarbon Support. *Small* **2021**, *17*, 2102288. [[CrossRef](#)]
21. Huang, H.; Chen, H.; Sun, D.; Wang, X. Graphene nanoplate-Pt composite as a high performance electrocatalyst for direct methanol fuel cells. *J. Power Sources* **2012**, *204*, 46–52. [[CrossRef](#)]
22. Nagasawa, K.; Takao, S.; Higashi, K.; Nagamatsu, S.-I.; Samjeské, G.; Imaizumi, Y.; Sekizawa, O.; Yamamoto, T.; Uruga, T.; Iwasawa, Y. Performance and durability of Pt/C cathode catalysts with different kinds of carbons for polymer electrolyte fuel cells characterized by electrochemical and in situ XAFS techniques. *Phys. Chem. Chem. Phys.* **2014**, *16*, 10075–10087. [[CrossRef](#)]
23. Padgett, E.; Yarlagadda, V.; Holtz, M.E.; Ko, M.; Levin, B.D.A.; Kukreja, R.S.; Ziegelbauer, J.M.; Andrews, R.N.; Ilavsky, J.; Kongkanand, A.; et al. Mitigation of PEM Fuel Cell Catalyst Degradation with Porous Carbon Supports. *J. Electrochem. Soc.* **2019**, *166*, F198–F207. [[CrossRef](#)]
24. Hernández-Fernández, P.; Montiel, M.; Ocón, P.; de la Fuente, J.L.G.; García-Rodríguez, S.; Rojas, S.; Fierro, J.L.G. Functionalization of multi-walled carbon nanotubes and application as supports for electrocatalysts in proton-exchange membrane fuel cell. *Appl. Catal. B Environ.* **2010**, *99*, 343–352. [[CrossRef](#)]
25. Guha, A.; Lu, W.; Zawodzinski, T.A.; Schiraldi, D.A. Surface-modified carbons as platinum catalyst support for PEM fuel cells. *Carbon* **2007**, *45*, 1506–1517. [[CrossRef](#)]
26. Comignani, V.; Sieben, J.M.; Sanchez, M.D.; Duarte, M.M.E. Influence of carbon support properties on the electrocatalytic activity of PtRuCu nanoparticles for methanol and ethanol oxidation. *Int. J. Hydrogen Energy* **2017**, *42*, 24785–24796. [[CrossRef](#)]
27. Acharya, C.K.; Li, W.; Liu, Z.; Kwon, G.; Turner, C.H.; Lane, A.M.; Nikles, D.; Klein, T.; Weaver, M. Effect of boron doping in the carbon support on platinum nanoparticles and carbon corrosion. *J. Power Sources* **2009**, *192*, 324–329. [[CrossRef](#)]
28. Perazzolo, V.; Brandiele, R.; Durante, C.; Zerbetto, M.; Causin, V.; Rizzi, G.A.; Cerri, I.; Granozzi, G.; Gennaro, A. Density Functional Theory (DFT) and Experimental Evidences of MetalSupport Interaction in Platinum Nanoparticles Supported on Nitrogen- and Sulfur-Doped Mesoporous Carbons: Synthesis, Activity, and Stability. *ACS Catal.* **2018**, *8*, 1122–1137. [[CrossRef](#)]
29. Kim, Y.-T.; Mitani, T. Competitive effect of carbon nanotubes oxidation on aqueous EDLC performance: Balancing hydrophilicity and conductivity. *J. Power Sources* **2006**, *158*, 1517–1522. [[CrossRef](#)]
30. Schmies, H.; Hornberger, E.; Anke, B.; Jurzinsky, T.; Nong, H.N.; Dionigi, F.; Kühl, S.; Drnec, J.; Lerch, M.; Cremers, C.; et al. Impact of Carbon Support Functionalization on the Electrochemical Stability of Pt Fuel Cell Catalysts. *Chem. Mater.* **2018**, *30*, 7287–7295. [[CrossRef](#)]
31. Kim, J.H.; Yuk, Y.; Joo, H.S.; Cheon, J.Y.; Choi, H.S.; Joo, S.H.; Park, J.Y. Nanoscale adhesion between Pt nanoparticles and carbon support and its influence on the durability of fuel cells. *Curr. Appl. Phys.* **2015**, *15*, S108–S114. [[CrossRef](#)]

32. Fang, Z.; Lee, M.S.; Kim, J.Y.; Kim, J.H.; Fuller, T.F. The Effect of Carbon Support Surface Functionalization on PEM Fuel Cell Performance, Durability, and Ionomer Coverage in the Catalyst Layer. *J. Electrochem. Soc.* **2020**, *167*, 064506. [CrossRef]
33. Niu, G.; Zhou, M.; Yang, X.; Park, J.; Lu, N.; Wang, J.; Kim, M.J.; Wang, L.; Xia, Y. Synthesis of PtNi Octahedra in Continuous-Flow Droplet Reactors for the Scalable Production of Highly Active Catalysts toward Oxygen Reduction. *Nano Lett.* **2016**, *16*, 3850–3857. [CrossRef] [PubMed]
34. Liao, T.-W.; Yadav, A.; Ferrari, P.; Niu, Y.; Wei, X.-K.; Vernieres, J.; Hu, K.-J.; Heggen, M.; Borkowski, R.E.D.; Palmer, R.E.; et al. “Composition-Tuned Pt-Skinned PtNi Bimetallic Clusters as Highly Efficient Methanol Dehydrogenation Catalysts. *Chem. Mater.* **2019**, *31*, 10040–10048. [CrossRef]
35. Spadaro, M.C.; Humphrey, J.J.L.; Cai, R.; Martínez, L.; Haigh, S.J.; Huttel, Y.; Spencer, S.J.; Wain, A.J.; Palmer, R. Electrocatalytic Behavior of PtCu Clusters Produced by Nanoparticle Beam Deposition. *J. Phys. Chem. C* **2020**, *124*, 23683–23689. [CrossRef] [PubMed]
36. Ayodele, O.B.; Cai, R.; Wang, J.; Ziouani, Y.; Liang, Z.; Spadaro, M.C.; Kovnir, K.; Arbiol, J.; Akola, J.; Palmer, R.E.; et al. Synergistic Computational–Experimental Discovery of Highly Selective PtCu Nanocluster Catalysts for Acetylene Semihydrogenation. *ACS Catal.* **2020**, *10*, 451–457. [CrossRef]
37. Liu, H.; Zhao, J.; Li, X. Controlled Synthesis of Carbon-Supported Pt-Based Electrocatalysts for Proton Exchange Membrane Fuel Cells. *Electrochem. Energy Rev.* **2022**, *5*, 13. [CrossRef]
38. Rodríguez-reinoso, F. The role of carbon materials in heterogeneous catalysis. *Carbon* **1998**, *36*, 159–175. [CrossRef]
39. Ott, S.; Orfanidi, A.; Schmies, H.; Anke, B.; Nong, H.N.; Hübner, J.; Gernert, U.; Gliech, M.; Lerch, M.; Strasser, P. Ionomer distribution control in porous carbon-supported catalyst layers for high-power and low Pt-loaded proton exchange membrane fuel cells. *Nat. Mater.* **2020**, *19*, 77–85. [CrossRef]
40. Xia, B.Y.; Wu, H.B.; Yan, Y.; Lou, X.W.D.; Wang, X. Ultrathin and Ultralong Single-Crystal Platinum Nanowire Assemblies with Highly Stable Electrocatalytic Activity. *J. Am. Chem. Soc.* **2013**, *135*, 9480–9485. [CrossRef]
41. Tan, X.; Shahgaldi, S.; Li, X. The effect of non-spherical platinum nanoparticle sizes on the performance and durability of proton exchange membrane fuel cells. *Adv. Appl. Energy* **2021**, *4*, 100071. [CrossRef]
42. Xia, B.Y.; Wu, H.B.; Yan, Y.; Wang, H.B.; Wang, X. One-Pot Synthesis of Platinum Nanocubes on Reduced Graphene Oxide with Enhanced Electrocatalytic Activity. *Small* **2014**, *10*, 2336–2339. [CrossRef]
43. Soboleva, T.; Zhao, X.; Malek, K.; Xie, Z.; Navessin, T.; Holdcroft, S. On the Micro-, Meso-, and Macroporous Structures of Polymer Electrolyte Membrane Fuel Cell Catalyst Layers. *ACS Appl. Mater. Interfaces* **2010**, *2*, 375–384. [CrossRef] [PubMed]
44. U.S. Department of Energy Multi-Year Research, Development, and Demonstration Plan: 3.4 Fuel Cells; 2017. Available online: https://www.energy.gov/sites/default/files/2017/05/f34/fcto_myrrdd_fuel_cells.pdf (accessed on 4 October 2021).
45. Inagaki, M.; Toyoda, M.; Soneda, Y.; Morishita, T. Nitrogen-doped carbon materials. *Carbon* **2018**, *132*, 104–140. [CrossRef]
46. Hornberger, E.; Merzdorf, T.; Schmies, H.; Hübner, J.; Klingenhof, M.; Gernert, U.; Kroschel, M.; Anke, B.; Lerch, M.; Schmidt, J.; et al. Impact of Carbon N-Doping and Pyridinic-N Content on the Fuel Cell Performance and Durability of Carbon-Supported Pt Nanoparticle Catalysts. *ACS Appl. Mater. Interfaces* **2022**, *14*, 18420–18430. [CrossRef] [PubMed]
47. Liu, Y.; Chen, H.; Tian, C.; Geng, D.; Wang, D.; Bai, S. One-Pot Synthesis of Highly Efficient Carbon-Supported Polyhedral Pt3Ni Alloy Nanoparticles for Oxygen Reduction Reaction. *Electrocatalysis* **2019**, *10*, 613–620. [CrossRef]
48. Lim, M. Development of Non-Spherical Platinum Catalyst with Functionalized Carbon Supports for Proton Exchange Membrane Fuel Cells. Master’s Thesis, University of Waterloo, Waterloo, ON, Canada, 2023.
49. Shahgaldi, S.; Zhao, J.; Alaefour, I.; Li, X. Investigation of catalytic vs reactant transport effect of catalyst layers on proton exchange membrane fuel cell performance. *Fuel* **2017**, *208*, 321–328. [CrossRef]
50. Pérez-Rodríguez, S.; Pastor, E.; Lázaro, M.J. Electrochemical behavior of the carbon black Vulcan XC-72R: Influence of the surface chemistry. *Int. J. Hydrogen Energy* **2018**, *43*, 7911–7922. [CrossRef]
51. Shinozaki, K.; Morimoto, Y.; Pivovar, B.S.; Kocha, S.S. Suppression of oxygen reduction reaction activity on Pt-based electrocatalysts from ionomer incorporation. *J. Power Sources* **2016**, *325*, 745–751. [CrossRef]
52. Speder, J.; Zana, A.; Spanos, I.; Kirkensgaard, J.J.K.; Mortensen, K.; Hanzlik, M.; Arenz, M. Comparative degradation study of carbon supported proton exchange membrane fuel cell electrocatalysts the influence of the platinum to carbon ratio on the degradation rate. *J. Power Sources* **2014**, *261*, 14–22. [CrossRef]
53. Labata, M.F.; Li, G.; Ocon, J.; Chuang, P.-Y.A. Insights on platinum-carbon catalyst degradation mechanism for oxygen reduction reaction in acidic and alkaline media. *J. Power Sources* **2021**, *487*, 229356. [CrossRef]

Disclaimer/Publisher’s Note: The statements, opinions and data contained in all publications are solely those of the individual author(s) and contributor(s) and not of MDPI and/or the editor(s). MDPI and/or the editor(s) disclaim responsibility for any injury to people or property resulting from any ideas, methods, instructions or products referred to in the content.